1 SELECTION OF THE MINIMAL TIME STEPS

The goal in this section is to determine the sufficient time-stepping scheme to resolve halo positions and masses reliably for the future galaxy surveys. We are particularly interested in reducing the number of sub-cycles, because most of computational time is spent in the short-range time solver. In order to quantitatively evaluate different time-stepping schemes, we run a set of convergence tests using smaller simulation boxes. As already explained, our aim is to carry out simulations in approximate $(4h^{-1}\mathrm{Gpc})^3$ volumes with 4096^3 particles, leading to a particle mass of $\tilde{}10^{11}\mathrm{M}_\odot$. We scales down these volumes to $(256h^{-1}\mathrm{Mpc})^3$ with 256^3 particles, which keeps the particle mass unchanged. In addition, we have carried out one simulation with 512^3 particles with exactly the same phases for detailed mass resolution studies. The number of time steps were chosen as 450/5, 300/3, 300/2, 150/3, 150/2, where the first number indicates the long time steps and the second number the number of short time steps for each long time step. Note that all the samples used in this section are at redshift $z = 0.15$. After determining our target time-stepping scheme, we do more detailed examination at various redshifts in the next section. To provide some idea of the variation across all of the choices, we compare observable quantities including mass functions and power spectra in real and redshift spaces, as well as masses and positions of halos matched one by one. Based on a number of convergence tests, the 300/2 combination turned out to be the final target.

1.1 Observables

We investigate how mass resolution and the number of time steps affect to observable quantities including mass functions and power spectra.

1.1.1 Mass Resolution

Here, we compare samples with 256^3 and 512^3 particles with the same initial conditions and the same number of time steps of 450/5. We first show comparison of cumulative mass functions in Figure 1. We calculate mean and its error through the bootstrap method, generating 100 samples by choosing halos randomly from an output of the simulation. The mean and its error for the samples of 512^3 particles are indicated as shaded regions in the right panel of Figure 1. The mean for 256^3 particles indicated as circles is within the error of 512^3 particles on halo masses $\tilde{}10^{13.5}\mathrm{M}_\odot$. The discrepancy in the mass functions between 256^3 particles and 512^3 particles becomes larger on large halo masses, mainly because there are a few large halos and therefore sensitive to differences in the number of halos. We also see that agreement between the samples of those two mass resolutions is better at lower redshift, possibly because particles are more well clustered at lower redshift. Those differences on mass functions can cause systematic errors on halo bias due to selection of halos. We compare halo auto power spectra to see how halo biases for those two mass resolusions can be differ in Figure 2. Figure 2 shows the ratio of auto power spectra in real-space for the simulations with 256^3 and 512^3 particles at three different redshifts, $z = 0.15$, $z = 0.5$, and $z = 0.8$. We subtract a Poisson shot noise of $1/n$, where n is the average number density of halos, to calculate the auto power spectra. The difference between auto power spectra of 256^3 and 512^3 particles is within 10% at any redshifts.

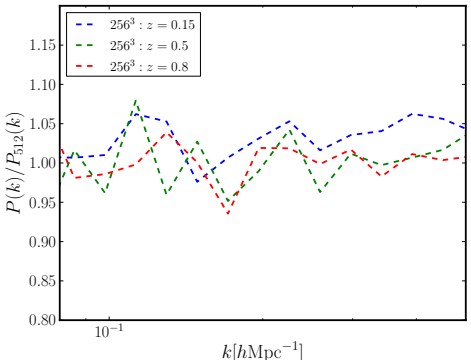

Figure 2. Ratio of halo auto power spectra between the samples of 512^3 and 256^3 particles for various redshifts. The agreements are all within 10%.

We also show the ratio of redshift-space power spectra in Figure 3. Since those ratios in real space and redshift space, it implies that measurements of the growth factor through redshift-space distortions will not significantly affected by mass resolusions of the siulations.

1.1.2 Time Steps

We first compute mass functions from outputs of different time-stepping schemes, as shown in

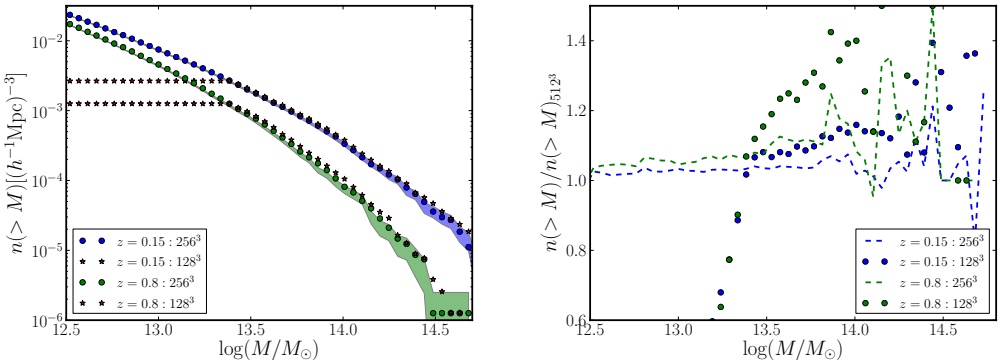

Figure 1. Left: Cumulative mass functions for the simulations of 512^3 and 256^3 particles. Shaded regions are the mean with errors for the samples of 512^3 particles calculated through the bootstrap method. Circles are the mean for 256^3 particles. Right: Ratio of cumulative mass functions between the samples of 512^3 and 256^3 particles. The deviation from on on large halo masses is mainly due to the fewer number of large halos.

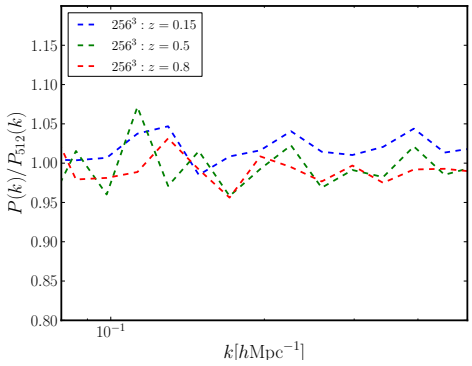

Figure 3. Ratio of redshift-space power spectra for various redshifts. The agreements are all within 10%. We find that the difference in power spectra are almost the same for both rea; and redshift spaces, implying that this difference in the power spectra is due to halo bias not from velocity fields.

Figure 4, where we compare simulations with reduced number of time steps to the 450/5 simulation. In Figure 4, we show the ratio $n(>M)/n_{450/5}(>M)$, where $n_{450/5}(>M)$ is a cumulative mass function for the 450/5 simulation and $n(>M)$ is a cumulative mass function for different time steps corresponding to different colors. Here, we use a fixed linking length of $b = 0.16$ times the mean interparticle separation for all the simulations to declare halos through the friends-of-friends (hereafter, fof) algorithm, and halo masses are assigned based on the number of particles contained in halos. We see that cumulative mass functons for 150 global steps have overall smaller amplitudes than 450 and 300 global steps. This is because smaller number of time steps make halos more diffused and the fixed linking length cannot connect some particles in the outputs of 150 global steps whose corresponding particles are connected in the simulations of larger global steps. In addition to the difference in global steps, sub-cycles also make an internal structure of halos more diffused and this leads to the suppression on the number of low-mass halos. In Manera et al. 2012 which uses the second-order Lagrangian perturbation theory to generate dark matter fields, they used a longer linking length and reassigned halo masses in order to solve the same problem of having diffused halos. We find that overall agreement between the simulations of 450/5 and 300 global steps on mass functions is sufficient.

The next statistics of interest is cross power spectra between halos and matter densities, as shown in Figure 5. Figure 5 shows the ratio $P_{hm}/P_{hm,450/5}$ at $z = 0.15$, where $P_{hm,450/5}$ is the cross power spectrum for 450/5 and P_{hm} is the cross power spectrum for other time steps labeled in the figure. To calculate the cross power spectra, we use the output of the 450/5 simulation for the matter densities for all the halo sample. In this way, the ratio $P_{hm}/P_{hm,450/5}$ is equivalent to the ratio of halo bias between the 450/5 and other time-steps, showing systematic errors due to the de-tuned simulations. Note that halos used here have the mass of $10^{12.5}\mathrm{M}_\odot$ to $10^{13.0}\mathrm{M}_\odot$, but we observed the same trend in cross power specra

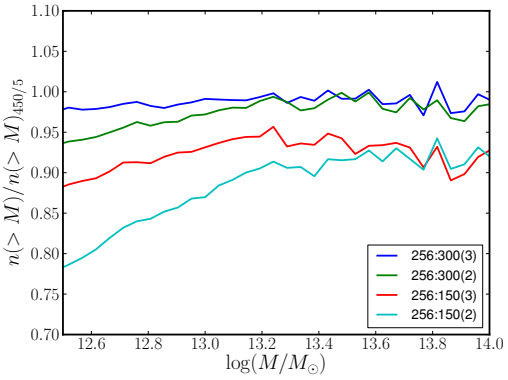

Figure 4. Comparison of cumulative mass functions in different simulations taking the 450/5 as a referene. Lines, from top to bottom, correspond to diferent time steps, 300/3 (blue), 300/2 (green), 150/3 (red), and 150/2 (cyan) respectively. As shown, the agreement between 300 global steps and the 450/5 is close to one on large halo mass and sub-cycles make differences only on small halo mass.

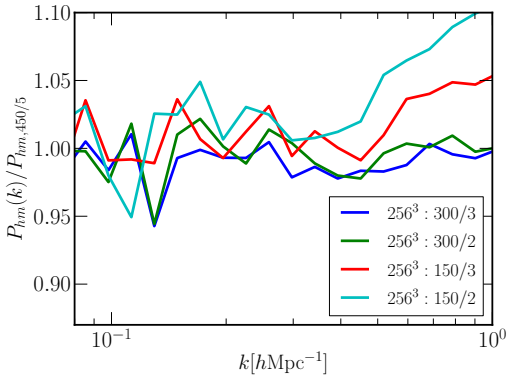

Figure 5. Ratio of halo-matter cross power spectra as a function of time steps with respect to the 450/5. The agreements with the 450/5 are all within 5% on large scales. For 300 global steps, both agree well even on small scales with little difference by sub-cycles.

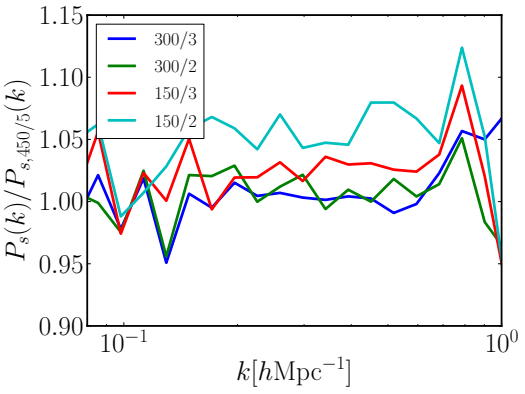

Figure 6. Ratio of redshift-space auto power spectra in different time steps, taking 450/5 as a reference. For 300 global steps, the agreement with the 450/5 is well within 5% on large scales.

calculated with different halo mass ranges. Here, we use only one realization for the calculations and this is partly why our cross power spectra are noisy on large scales. Other cause of this noisiness is the small volume of the simulation box. We see that the agreement between 450/5 and 300 global steps is remarkably well that the differences are well within 5% on any scales. Besides that, we see the systematic error on halo biases for 150 global steps is also within 5% on large scales. This implies that halo bias on large scales is not largely affected by reduction of time steps.

The final quantitative comparison here is auto power spectra in redshift space. We are particularly interested in how de-tuning affects to velocity fields and therefore to redshift space on large scales. The result is shown in Figure 6 as the ratio $P_s/P_{s,450/5}$, where $P_{s,450/5}$ is the auto power spectrum calculated from the simulation of 450/5 and P_s is the auto power spectrum with reduced number of time steps. Before taking the ratio, we subtracted a Poisson shot noise contribution of $1/n$. The mass threshold used here is $10^{12.5}\mathrm{M}_\odot$. We see that the simulations with 150 global steps do not have the same velocity fields as the 450/5 simulation, for the reason that their ratios for the redshift-space power spectra between 450/5 and 150 global steps have more discrepancy from one compared to the ratios for halo biases, shown in Figure 5. This implies that the simulations with 150 global steps cause systematics errors in measurement of the growth factor through redshift-space distortions. For 300 global steps, the agreement with the 450/5 simulation is sufficiently well on large scales.

1.2 Matching

We compare halo properties including statistically for corresponding halos in different samples. We first show our algorithm of indetifying corresponding halos in two different samples and then compare halo mass, position, and velocity for those matched halos. From the quantitative

comparison, we find that the samples with 300 global steps have much less scatter with the 450/5 sample, taken as a reference. In addition to that, we see that the differences between sub-cycles are almost negligible.

1.2.1 algorithm

Since our simulations all start with the same initial conditions, we match halos in different simulations by matching their particle content. Given a halo in simulation A, we consider the halos in simulation B that its particles correspond to. Given this list of possible matches, we match to the halo with the largest number of common particles. To avoid spurious matches, we also require that this fraction of common particles (relative to simulation A) exceeds a chosen threshold. Figure 7 Shows the cumulative fraction of unmatched halos matching the 450/5 to the 300/2 simulation at $z = 0.15$ with various thresholds. As expected, the unmatched fraction increases with increasing threshold and decreasing hao mass. We adopt a threshold of 50% as out default choice.

Since the above matching algorithm is unidirectional, multiple halos in A might be matched to a single halo in B; this happens 1 to 2% of the time with a matching threshold of 50%. We refer to these as multiply-booked halos in what follows. Figure 8 compares halo mass for the matched halos between the 450/5 and the 300/2 simulations at $z = 0.15$. We classified those matched halos into multiply-booked halos and the rest. As shown in Figure 8, the summed halo mass for those multiply-booked halos in the 450/5 is correlated with the corresponding halos in the 300/2 better than the individual halo mass in the 450/5. This inplies that those multiply-booked halos in the 450/5 are merged into one halo in the 300/2. Since larger global steps and sub-cycles can capture dynamics better, it is likely that the halos in the 450/5 forms sub-structure ealier than the 300/2 simulation.

Figure **??** shows the number densities of the unmatched halos in the 450/5 matching to the 300/2 at $z = 0.15$. There are three reasons that halos are considered as unmatched. First, if there are no common particles in the halos, we consider them as unmatched. Second, if the fraction of common particles over the total number of particles in each halo is less than 50%, we eliminate those spurious halos. At last, we remove the multiply-booked halos except the ones which have

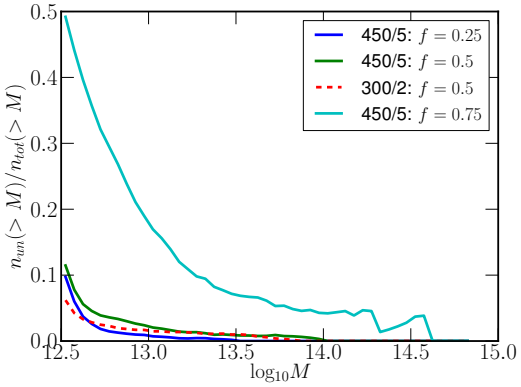

Figure 7. The cumulative fraction of unmatched halos matching the 450/5 to the 300/2 simulation at z=0.15 as a function of halo mass. The solid lines, from top to bottom, correspond to matching thresholds of 75%, 50%, and 25%. The dashed line shows the same quantity except now matching the 300/2 to the 450/5 simulation for a threshold of 50%. As expected, the unmatched fraction increases with decreasing halo mass and increasing threshold. We adopt a threshold of 50% as our default choice.

the most number of common particles. We showed each unmatched number density as a function of halo mass. There are only low-mass unmatched halos for not having any common particles. This is because low-mass halos are formed with smaller number of particles and it is likely that particles in a halo in A do not form a halo in B. As shown, most of unmatched halos are due to the threshold criterion.

At last, we show how our matching algorithm works for different redshifts and different time steps, shown in Figure 10. The left panel of Figure 10 shows cumulative fractions of unmatched halos matching the simulation of 300/2 to the 450/5 for various redshifts. As shown, we do not see any redshift dependence in the number of unmatched halos. In the right panel of Figure 10, we compare cumulative fractions of unmatched halos for various time steps at $z = 0.15$. As expected, fewer number of time steps increases the number of unmatched halos. It is possible that the simulations with fewer time steps do not resolve substructure of halos, creating more multiply-booked halos on large halo masses.

1.2.2 halo properties

Here, we present halo properties (i.e., halo mass, position, and velocity) for matched halos match-

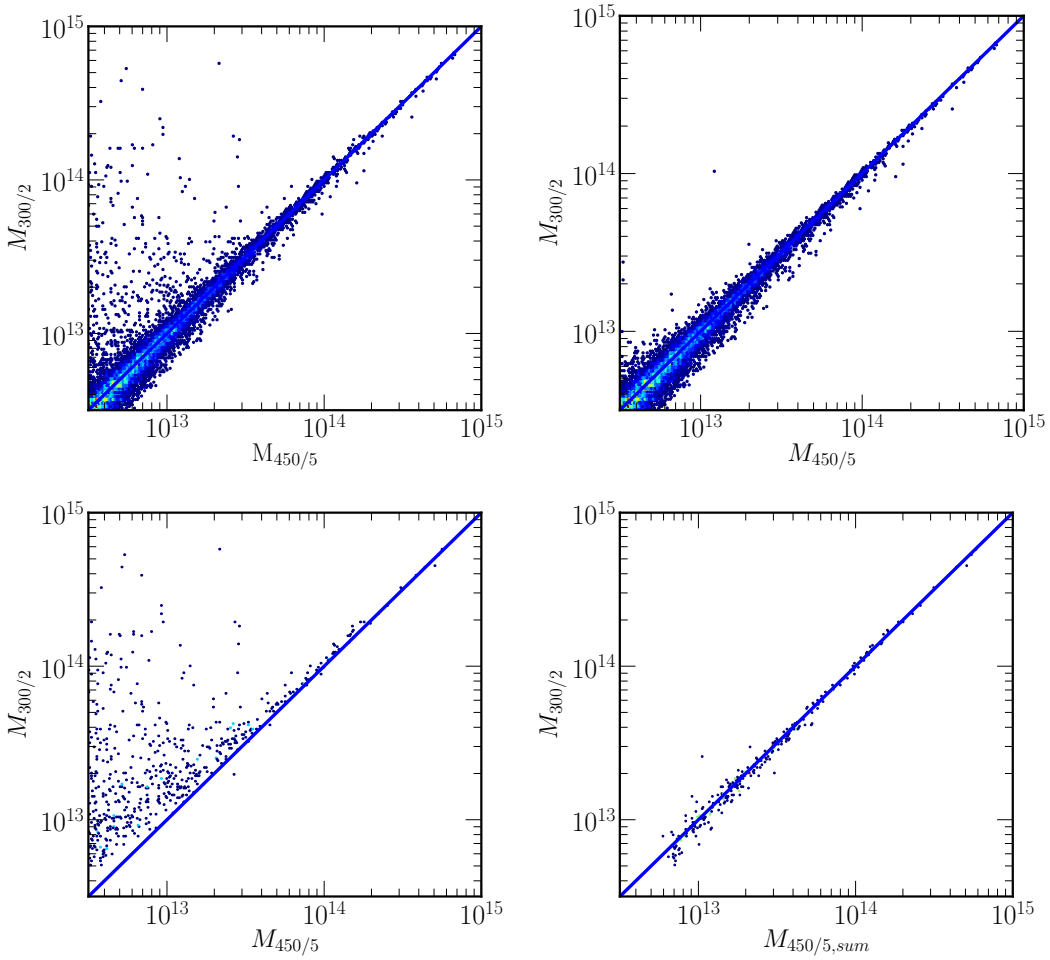

Figure 8. Comparison of halo masses matching the 450/5 (x-axis) to the 300/2 (y-axis) simulation at $z = 0.15$. Panels correspond to halos with different matching criteria: all the matched halos (top left), matched halos having one-to-one correspondence (top right), matched halos not having one-to-one correspondence called "multiply-booked" halos (bottom left), and the "multiply-booked" halos whose corresponding halo masses are added (bottom right). Those panels imply that large mass difference between the 450/5 and the 300/2 shown in the top left panel is mainly due to those "multiply-booked" halos and that the corresponding "multiply-booked" halos in the 450/5 are merged into one halo in the 300/2 due to larger time steps.

ing to the 450/5, taken as a reference. The panels in Figure 11, from left to right, show the comparison of halo mass, position, and velocity for the matched halos at $z = 0.15$. As shown, the 150 global steps have more scatter in the halo properties and the means are off from the center to the halo mass ratio and the velocity difference. This indicates that the halo structure in these cases is more diffused than the case of the 300 or the 450 global steps. For the 300 global steps, the results are siginificantly improved and the center position is matched in these cases to better than 200 kpc. As is clear from Figure 11, the difference between 3 and 2 sub-cycles is negligible on halo properties. The same results shown in Figure 11 but for other redshifts are in Table 1, 2,3, and 4, and they support the same argument discussed for Figure 11. Table 4 shows fractions of halos whose velocity directions are matched to the ones for the 450/5 within 10 degree. More than 90% of the matched halos have angles between the veloci-

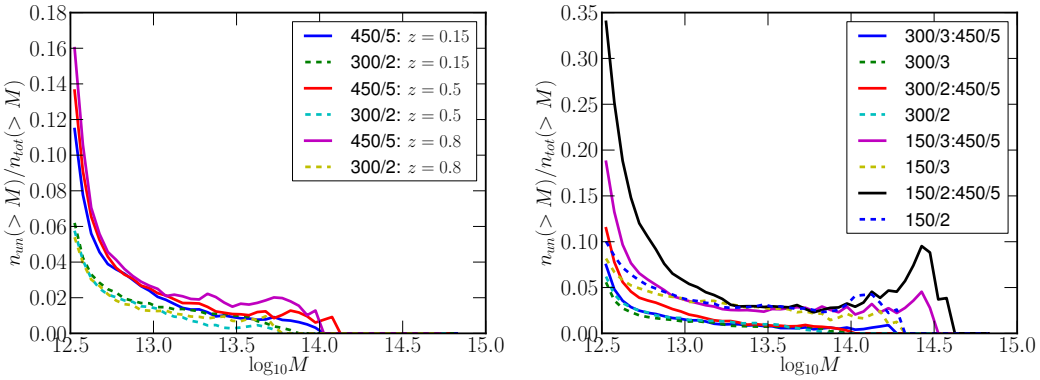

[p]

Figure 10. Right: The cumulative fraction of unmatched halos matching the 450/5 to the 300/2 as a function of redshift. Left: The cumulative fraction of unmatched halos matching the 450/5 to the other step sizes at $z = 0.15$.

[t]

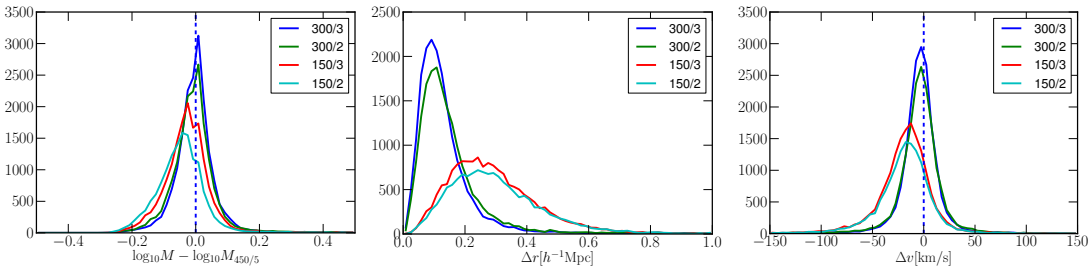

Figure 11. Comparison of matched halos in the different simulations corresponding to 300/3 (blue), 300/2 (green), 150/3 (red), and 150/2 (cyan) with respect to the 450/5. From left to right, we compared halo mass, position, and velocity respectively. or Comparison of matched halos in the different simulations corresponding to 300/3 (blue), 300/2 (green), 150/3 (red), and 150/2 (cyan). From left to right, we compare halo mass, position, and velocity for th halos matching to the 450/5 simulation respectively. The agreement between 300 global steps and the 450/5 is considerably well with little difference of sub-cycles.

ties within 10 degree at all the redshifts, $z = 0.15$, $z = 0.5$, and $z = 0.8$.

2 TUNING 300/2

*explain about the problem

2.1 method

2.2 Mass Function before and after

2.3 Power Spectra

*Should I also do redshift-space power spectra?

*We can also calculate redshift-space power spectra with different time steps for matter densities instead of halos. Theoretically, mass selection only affects to halo bias not not the growth factor...which means that this tweking should not affect to redshift-space halo power spectra more than halo bias...

[h] Table: $\log_{10}(M/M_{450/5})$

z=0.15	median	$\Delta_{65\%}$	$\Delta_{95\%}$
300/3	-0.0026	0.0877	0.2864
300/2	-0.0078	0.0972	0.3458
150/3	-0.0266	0.1107	0.3101
150/2	-0.0454	0.1207	0.3315

z=0.5	median	$\Delta_{65\%}$	$\Delta_{95\%}$
300/3	-0.0062	0.0905	0.2869
300/2	-0.0139	0.1029	0.3345
150/3	-0.0372	0.1148	0.3083
150/2	-0.0595	0.1252	0.3093

z=0.8	median	$\Delta_{65\%}$	$\Delta_{95\%}$
300/3	-0.0067	0.0932	0.2891
300/2	-0.0189	0.1048	0.3347
150/3	-0.0519	0.1172	0.2926
150/2	-0.0782	0.1274	0.28878

Table 1. Comparison of halo mass ratios $\log_{10}M/M_{450/5}$ in log-based, comparing various time steps to the 450/5 simulation at $z = 0.15$, $z = 0.5$, and $z = 0.8$. For each redshift, we report median, $\Delta_{95\%}$, and $\Delta_{65\%}$ (how should I explain about $\Delta_{95\%}$?). As shown in Figure 11, the results indicate that mass ratio distributions for the 300 global steps have less scatter than for the 150 global steps.

[H]

z=0.15	median	$\Delta_{65\%}$	$\Delta_{95\%}$
$M_{halo} \in [10^{12.5}, 10^{13.0}]$	-0.0111	0.1124	0.3896
$M_{halo} \in [10^{13.0}, 10^{13.5}]$	-0.0085	0.0748	0.2599
$M_{halo} \in [10^{13.5}, 10^{14.0}]$	-0.0056	0.0471	0.1596
$M_{halo} > 10^{14.0}$	-0.0047	0.0341	0.1323

z=0.5	median	$\Delta_{65\%}$	$\Delta_{95\%}$
$M_{halo} \in [10^{12.5}, 10^{13.0}]$	-0.0197	0.1156	0.3544
$M_{halo} \in [10^{13.0}, 10^{13.5}]$	-0.0123	0.0790	0.2546
$M_{halo} \in [10^{13.5}, 10^{14.0}]$	-0.0067	0.0497	0.1813
$M_{halo} > 10^{14.0}$	-0.0052	0.0309	0.0731

z=0.8	median	$\Delta_{65\%}$	$\Delta_{95\%}$
$M_{halo} \in [10^{12.5}, 10^{13.0}]$	-0.0260	0.1161	0.3478
$M_{halo} \in [10^{13.0}, 10^{13.5}]$	-0.0167	0.0835	0.2546
$M_{halo} \in [10^{13.5}, 10^{14.0}]$	-0.0084	0.0490	0.1809
$M_{halo} > 10^{14.0}$	-0.0077	0.0297	0.1361

Table 2. Comparison of halo mass ratios $\log_{10}M_{300/2}/M_{450/5}$ in log-based, comparing the 300/2 to the 450/5 simulation as a function of halo mass slices at $z = 0.15$, $z = 0.5$, and $z = 0.8$. For each redshift, we report median, $\Delta_{95\%}$, and $\Delta_{65\%}$. As shown, medians and Δs decreases as increasing halo mass and decreasing redshift.

[H]

z=0.15	median	$\Delta_{65\%}$	$\Delta_{95\%}$
300/3	0.1116	0.1228	0.4439
300/2	0.1245	0.1406	0.5558
150/3	0.2706	0.2571	0.6234
150/2	0.2800	0.2680	0.6568

z=0.5	median	$\Delta_{65\%}$	$\Delta_{95\%}$
300/3	0.1221	0.1298	0.4700
300/2	0.1348	0.1460	0.5400
150/3	0.2382	0.2248	0.5555
150/2	0.2475	0.2335	0.5835

z=0.8	median	$\Delta_{65\%}$	$\Delta_{95\%}$
300/3	0.1217	0.1329	0.4553
300/2	0.1354	0.1498	0.4969
150/3	0.2447	0.2284	0.5408
150/2	0.2536	0.2334	0.5418

Table 3. Comparison of halo positions for various time steps to the 450/5 simulation at $z = 0.15$, $z = 0.5$, and $z = 0.8$. For each redshift, we report median, $\Delta_{95\%}$, and $\Delta_{65\%}$. As shown, the halo positions for the 150 global steps are more scattered and 3 and 2 sub-cycles affect negligibly on halo positions. Also, there is little change due to redshift.

z=0.15	median	$\Delta_{65\%}$	$\Delta_{95\%}$
300/3	-3.36	24.3872	82.20
300/2	-3.26	27.5063	99.40
150/3	-16.61	38.4702	116.93
150/2	-17.05	39.9572	121.45

z=0.5	median	$\Delta_{65\%}$	$\Delta_{95\%}$
300/3	-3.78	36.87	118.48
300/2	-3.94	40.77	137.62
150/3	-23.25	53.41	151.75
150/2	-24.26	56.75	160.15

z=0.8	median	$\Delta_{65\%}$	$\Delta_{95\%}$
300/3	-6.32	47.41	149.72
300/2	-6.47	53.48	169.1556
150/3	-25.23	67.62	186.29
150/2	-24.76	71.97	189.26

Table 4. Comparison of halo velocity for various time steps to the 450/5 simulation at $z = 0.15$, $z = 0.5$, and $z = 0.8$. For each redshift, we report median, $\Delta_{95\%}$, and $\Delta_{65\%}$. As shown in Figure 11, the results indicate that mass ratio distributions for the 300 global steps have less scatter than for the 150 global steps.

z=0.15	fraction within 10 degree
300/3	0.951
300/2	0.938
150/3	0.928
150/2	0.923

Table 5. Fractions of halos whose velocity direction matches with the 450/5 within 10 degree at $z = 0.15$. More than 90% f halos for any time steps agree with the 450/5 simulation.